Computationally Efficient Receiver Design for Mitigating Multipath for Positioning with LTE Signals

Kimia Shamaei, Joe Khalife, Souradeep Bhattacharya, and Zaher M. Kassas
University of California, Riverside

BIOGRAPHIES

Kimia Shamaei is a Ph.D. candidate at the University of California, Riverside and a member of the Autonomous Systems Perception, Intelligence, and Navigation (ASPIN) Laboratory. She received her B.S. and M.S. in electrical engineering from the University of Tehran. Her current research interests include analysis and modeling of signals of opportunity and software-defined radio.

Joe J. Khalife is a Ph.D. student at the University of California, Riverside and a member of the ASPIN Laboratory. He received a B.E. in Electrical Engineering and an M.S. in Computer Engineering from the Lebanese American University (LAU). From 2012 to 2015, he was a research assistant at LAU. His research interests include opportunistic navigation, autonomous vehicles, and software-defined radio.

Souradeep Bhattacharya is an undergraduate student at the University of California, Riverside and a member of the ASPIN Laboratory. He is currently pursuing degrees in bioengineering and electrical engineering. His current research interests include software-defined radio, unmanned aerial vehicles, and embedded systems.

Zaher (Zak) M. Kassas is an assistant professor at the University of California, Riverside and director of the ASPIN Laboratory. He received a B.E. in Electrical Engineering from LAU, an M.S. in Electrical and Computer Engineering from The Ohio State University, and an M.S.E. in Aerospace Engineering and a Ph.D. in Electrical and Computer Engineering from The University of Texas at Austin. From 2004 through 2010 he was a research and development engineer with the LabVIEW Control Design and Dynamical Systems Simulation Group at National Instruments Corp. His research interests include cyber-physical systems, estimation theory, navigation, autonomous vehicles, and intelligent transportation systems.

ABSTRACT

A receiver for positioning with LTE signals, which could mitigate multipath in a computationally efficient fashion is presented. The receiver uses an orthogonal frequency division multiplexing (OFDM)–based delay-locked loop (DLL) to track the received LTE signals. The ranging error performance in an additive white Gaussian noise (AWGN) channel is evaluated numerically. The results demonstrate robust and accurate performance for high transmission LTE bandwidths. The proposed receiver is evaluated on a ground vehicle in an urban environment. Experimental results show a root mean squared error (RMSE) of 5.36 m, a standard deviation of 2.54 m, and a maximum error of 12.97 m between the proposed LTE receiver and the GPS navigation solution over a 1.44 Km trajectory. The robustness of the obtained pseudoranges with the proposed receiver are demonstrated against two algorithms: estimation of signal parameters by rotational invariance techniques (ESPRIT) and EKAT (ESPRIT and Kalman filter).

I. INTRODUCTION

Traditional approaches to address the limitations of global navigation satellite system (GNSS) have focused on fusing GNSS receivers with dead-reckoning systems and map-matching algorithms [1–3]. Over the past decade, a new paradigm has emerged to address GNSS limitations, which is to exploit ambient signals of opportunity (SOPs), such as cellular, digital television, AM/FM, WiFi, and iridium satellite signals [4–11]. Among the different SOPs, cellular signals are particularly attractive due to their ubiquity, geometric diversity, high received power, and large bandwidth [12]. Cellular signals can be exploited for localization to either produce a navigation solution in a standalone fashion [13, 14] or to aid the inertial navigation system (INS) in the absence of GNSS signals [15, 16]. Moreover, it has been demonstrated that fusing cellular signals with GNSS signals when available significantly improves the positioning accuracy [17, 18].

Preprint of the 2017 ION GNSS Conference Portland, OR, September 25–29, 2017

One of the main navigation sources of error that arises when using cellular signals is multipath. Received cellular signals experience more multipath than GNSS signals, particularly for ground-based receivers in urban canyons, due to the low elevation angles at which signals are received [19]. High transmission bandwidth signals could resolve multipath, making cellular long-term evolution (LTE) signals attractive due to their large bandwidth (up to 20 MHz).

The positioning performance achieved with LTE signals has been analyzed in the literature [20–23] and several software-defined receivers (SDRs) have been proposed for navigation with real and laboratory-emulated LTE signals [24–26]. Experimental results demonstrated navigation solutions with different types of LTE reference signals in different environments, achieving meter level accuracy [12, 19, 26–28].

The cell-specific reference signal (CRS) is one of the possible reference sequences in the received LTE signal that has been shown to yield accurate positioning when exploited due to its large transmission bandwidth [19]. Its high bandwidth (up to 20 MHz) enables resolving the line-of-sight (LOS) signal from multipath signals in the environment. The CRS is transmitted to estimate the channel between the LTE base station (also known as Evolved Node B or eNodeB) and the user equipment (UE).

The CRS is scattered in the bandwidth and is transmitted in multiple symbols of the LTE frame, making the usage of computationally inexpensive delay-locked loops (DLLs) for tracking the signal infeasible. Several non-DLL-based approaches have been proposed. A super resolution algorithm (SRA)–based technique was developed in [29, 30] to obtain the best case performance for positioning with the CRS. While this method provided meter level accuracy, it was computationally expensive and not suitable for real-time implementation. A first peak detection was proposed in [24, 26] to obtain the time-of-arrival (TOA) using the CRS. While this method is computationally inexpensive, it is impractical to detect the first peak of the channel impulse response when the multipath has short range.

This paper proposed a novel receiver that deals with the shortcomings of the SRA-based and first-peak-detection-based receivers. The proposed receiver is computationally-efficient and robust to multipath effects. A specialized orthogonal frequency division multiplexing (OFDM)–based DLL is designed to track the CRS signals. The performance of this receiver is compared against two methods: estimation of signal parameters by rotational invariance techniques (ESPRIT) [31] and EKAT (ESPRIT and Kalman filter) [30]. The comparison is made in terms of the accuracy of the produced pseudoranges and implementation cost.

The remainder of this paper is organized as follows. Section II presents a brief review of the LTE signal structure and transmission signal model. Section III discusses the receiver architecture. Section IV presents the experimental results for a ground vehicle navigating exclusively with real LTE signals and compares the proposed receiver against the ESPRIT and EKAT algorithms. Section V concludes the paper.

II. LTE SIGNAL MODEL

In this section, the structure of the LTE signals is first discussed. Then, the signals that can be used for positioning in LTE systems are provided. Finally, the received signal model is presented.

A. Frame Structure

In OFDM, which is used in the LTE downlink transmission, the serial data symbols are first divided into groups of length N_r. Then, each group is parallelized, zero-padded to length N_c, and an inverse fast Fourier transform (IFFT) is taken, resulting in an OFDM symbol. The last L_{CP} elements of the symbol are repeated at the beginning to provide the cyclic prefix (CP) and are used to suppress the interference due to multipath. A symbol has duration of $T_{symb} = 1/\Delta f$, where $\Delta f = 15$ KHz is the subcarrier spacing. In LTE systems, the values of N_r and N_c, which represent the bandwidth W (in MHz), are not unique and can be assigned to [32]

$$(N_r, N_c, W) = \big\{(72, 128, 1.4), (180, 256, 3), (300, 512, 5), (600, 1024, 10), (900, 1536, 15), (1200, 2048, 20)\big\}.$$

The resulting OFDM symbols are grouped into frames with a duration of 10 ms. In frequency-division duplexing (FDD) transmission, each frame is divided into 20 slots with a duration of 0.5 ms. Each slot with a normal CP allocation contains seven OFDM symbols. In a normal CP allocation, the CP of the first symbol of each slot has duration of 5.21 μs and the rest of the symbols' CPs have a duration of 4.69 μs.

B. Ranging Signals

In every LTE frame, two signals namely the primary synchronization signal (PSS) and the secondary synchronization signal (SSS), are transmitted to provide the frame start time to the UE. The PSS is a Zadoff-Chu sequence of length 62, which is transmitted on the last symbols of slots 0 and 10. The PSS is transmitted in one form of three possible sequences, each of which maps to an integer representing the sector ID of the eNodeB, i.e., $N_{ID}^{(2)} \in \{0, 1, 2\}$.

The SSS is also an orthogonal sequence of length 62, which is transmitted on the sixth symbol of slot 0 or 10. This orthogonal sequence is defined based on $N_{ID}^{(2)}$ and the slot number in which the SSS is transmitted. The SSS is transmitted in one of 168 possible forms, each of which maps to an integer representing the eNodeB's group identifier, i.e., $N_{ID}^{(1)} \in \{0, \cdots, 167\}$. By knowing $N_{ID}^{(1)}$ and $N_{ID}^{(2)}$, the UE can obtain the eNodeB's cell ID as [32]

$$N_{ID}^{Cell} = 3 \times N_{ID}^{(1)} + N_{ID}^{(2)}.$$

The CRS is another transmitted signal, which can be used for ranging. The CRS, which is scattered in time and bandwidth, is transmitted for channel estimation purposes. The CRS is an orthogonal sequence, which is defined based on the cell ID, the allocated symbol, slot, and the transmission antenna port number. The eNodeB's cell ID indicates the designated subcarriers to the CRS. In this paper, the CRS transmitted on the i-th symbol is denoted by $S_i(m)$, where $m = 0, \cdots, M-1$, $M = \lfloor N_r/\Delta_{CRS} \rfloor$, and $\Delta_{CRS} = 6$. The subcarriers allocated to $S_i(m)$ are $k = m\Delta_{CRS} + \nu_{i,N_{ID}^{Cell}}$, where $\nu_{i,N_{ID}^{Cell}}$ is a constant shift depending on the cell ID and i.

C. Received Signal Models

It is assumed that the i-th OFDM symbol is transmitted in a multipath fading channel, which stays constant over the duration of a symbol and has the channel impulse response

$$h_i(\tau) = \sum_{l=0}^{L-1} \alpha_i(l)\, \delta(\tau - \tau_i(l)),$$

where L is the number of multipath components; $\alpha_i(l)$ and $\tau_i(l)$ are the relative attenuation and delay components, respectively, of the l-th path with respect to the first path; $\alpha_i(0) = 1$ and $\tau_i(0) = 0$; and δ is the Dirac delta function. Therefore, the i-th received symbol after removing the CP and taking a fast Fourier transform (FFT) in a perfect synchronization condition will be

$$R_i'(k) = \sqrt{C}\, Y_i(k) H_i(k) + W_i(k), \quad \text{for } k = 0, \cdots, N_c - 1,$$

where $Y_i(k)$ is the i-th transmitted OFDM symbol, C is the received signal power due to the antenna gain and any implementation loss, $W_i(k) \sim \mathcal{CN}(0, \sigma^2)$, and

$$H_i(k) = \sum_{l=0}^{L-1} \alpha_i(l) e^{-j2\pi\tau_i(l)k/T_{symb}} \tag{1}$$

is the channel frequency response. In general, there is a mismatch between the estimated received symbol timing and the actual one, which can be due to imperfect synchronization or clock drift. Assuming that this mismatch is less than the CP duration, the received signal can be rewritten as

$$R_i'(k) = e^{j2\pi e_\theta k/N_c} \sqrt{C}\, Y_i(k) H_i(k) + W_i(k), \quad \text{for } k = 0, \cdots, N_c - 1, \tag{2}$$

where $e_\theta = \hat{\theta} - \theta$ represents the symbol timing error normalized by the sampling interval $T_s = T_{symb}/N_c$, and $\hat{\theta}$ and θ are the normalized estimated and true symbol timings, respectively.

III. RECEIVER ARCHITECTURE

The structure of the proposed LTE SDR is shown in Fig. 1. As can be seen in Fig. 1, the nodes A and B can switch between 1, 2, and 3. This connection is assigned based on the stage in which the receiver is operating. In the first stage, where A and B are connected to 1, the receiver obtains a coarse estimate of the frame start time by acquiring the PSS and SSS. In the second stage, where A and B are connected to 2, the receiver refines the initial estimate using the ESPRIT algorithm. In the last stage, where A and B are connected to 3, the receiver tracks the signal in which a fine estimate of the TOA is obtained. Each stage is discussed in details the following subsections.

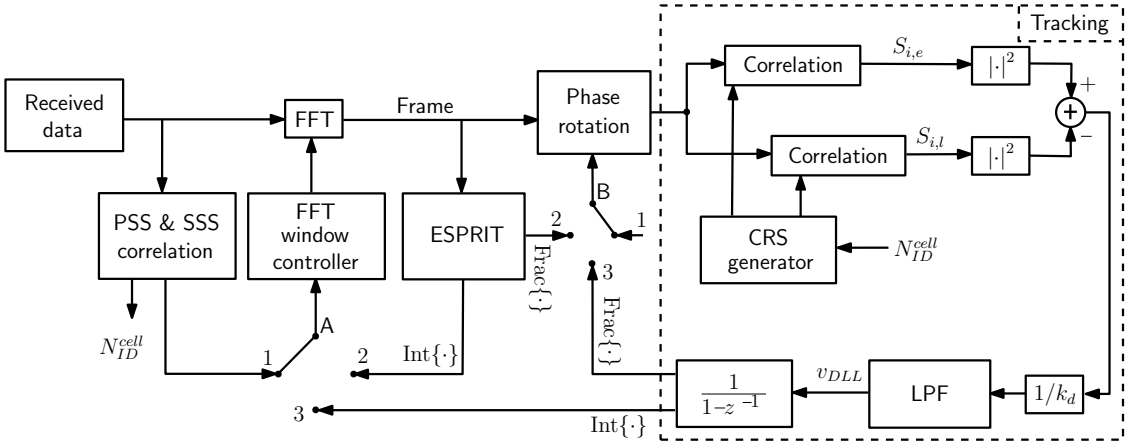

Fig. 1. Block diagram of the proposed LTE receiver architecture.

A. Stage 1: Initial Acquisition

In the first stage, a coarse estimate of the frame start time is obtained. This enables the receiver to convert the received signal into a frame structure. For this purpose, the UE first correlates the received signal with the locally generated time-domain PSS signal [26]. The peak of the correlation result shows the position of the PSS, which can be used for obtaining the symbol timing. Then, the signal is correlated with the locally generated time-domain SSS signal. The correlation result is used to estimate the frame start time and to calculate the cell ID. The PSS and SSS have approximately 1 MHz bandwidth; therefore, the peak of the correlations may have a bias compared to the true frame timing in a multipath environment.

Knowing the coarse estimate of the frame start time, the LTE signal can be converted into the frame structure by removing the CPs and taking an FFT. Assuming that the bias in the frame start time estimation is less than the CP length, the received signal model follows (2).

B. Stage 2: Acquisition Refinement

In the second stage, the symbol timing error, e_θ, is estimated using the ESPRIT algorithm. The details of this method are discussed in [30]. The normalized estimated symbol timing error, $\hat{e}_\theta$, can be divided into two parts: integer, $\text{Int}\{\cdot\}$, and fractional, $\text{Frac}\{\cdot\}$, given by

$$\hat{e}_\theta = \text{Int}\{\hat{e}_\theta\} + \text{Frac}\{\hat{e}_\theta\},$$

where $-1 \leq \text{Frac}\{\hat{e}_\theta\} \leq 0$. The integer part is used to control the FFT window, and the fractional part is removed from the signal using a phase rotation in R_i' as

$$R_i(k) = e^{-j2\pi k/N_c \text{Frac}\{\hat{e}_\theta\}} R_i'(k).$$

Therefore, the remaining symbol timing error will be

$$\tilde{e}_\theta = e_\theta - \hat{e}_\theta,$$

and the i-th received symbol on the subcarriers carrying the CRS can be written as

$$R_i(k) = e^{j2\pi m/M \tilde{e}_\theta} \sqrt{C} S_i(m) H_i(k) + W_i(k), \quad \text{for} \quad k = m\Delta_{CRS} + \nu_{i,N_{ID}^{Cell}}, \quad m = 0, \cdots, M-1.$$

C. Stage 3: Tracking

In the third stage, a DLL is used to track the symbol timing. In conventional DLLs (e.g., dot-product) the TOA error is obtained as a function of the early, late, and prompt correlations, which are the correlation of the received signals with locally generated early (advanced), late (delayed), and prompt versions of the code sequence, respectively. The

CRS is scattered in the bandwidth, which makes obtaining its time-equivalent form infeasible. As a result, obtaining the time-domain correlation of the received signal and the code will not be possible and conventional DLLs cannot be used to track the CRS. In this paper, a specialized DLL will be designed specifically for tracking the CRS in LTE systems. This DLL is an adaptation of [33] for OFDM systems.

Since a shift in the time-domain is equivalent to a phase rotation in the frequency-domain, the locally generated early and late code signals for the i-th OFDM symbol can be obtained respectively as

$$R_{i,e}(m) = e^{-j2\pi m/M\xi} S_i(m),$$
$$R_{i,l}(m) = e^{j2\pi m/M\xi} S_i(m),$$

where $m = 0, 1, \cdots, M-1$ and $0 < \xi \leq 1/2$ is the normalized time shift. The early and late correlations in the frequency-domain can be expressed respectively as

$$S_{i,e} = \sum_{m=0}^{M-1} R_i(m\Delta_{CRS} + \nu_{i,N_{ID}^{Cell}}) R_{i,e}^*(m),$$
$$S_{i,l} = \sum_{m=0}^{M-1} R_i(m\Delta_{CRS} + \nu_{i,N_{ID}^{Cell}}) R_{i,l}^*(m).$$

The discriminator function is defined as

$$D_i \triangleq |S_{i,e}|^2 - |S_{i,l}|^2 \triangleq M^2 C S_d(\tilde{e}_\theta, \xi) + N_{i,d},$$

where for a channel without multipath, $S_d(\tilde{e}_\theta, \xi)$ is the normalized S-curve function defined as

$$S_d(\tilde{e}_\theta, \xi) = \left\{ \left(\frac{\sin(\pi(\tilde{e}_\theta - \xi))}{M \sin(\pi(\tilde{e}_\theta - \xi)/M)} \right) - \left(\frac{\sin(\pi(\tilde{e}_\theta + \xi))}{M \sin(\pi(\tilde{e}_\theta + \xi)/M)} \right) \right\},$$

and $N_{i,d}$ represents the noise with zero-mean and variance [33]

$$\text{var}[N_{i,d}] \leq 2M^2\sigma^4 \left[1 + \frac{C}{M\sigma^2} \left(\frac{\sin(\pi(\tilde{e}_\theta - \xi))}{\sin(\pi(\tilde{e}_\theta - \xi)/M)} \right)^2 + \frac{C}{M\sigma^2} \left(\frac{\sin(\pi(\tilde{e}_\theta + \xi))}{\sin(\pi(\tilde{e}_\theta + \xi)/M)} \right)^2 \right],$$

where equality holds for $\xi = 0.5$. In the following analysis, ξ is set to be 0.5. Fig. 2 shows the normalized S-curve.

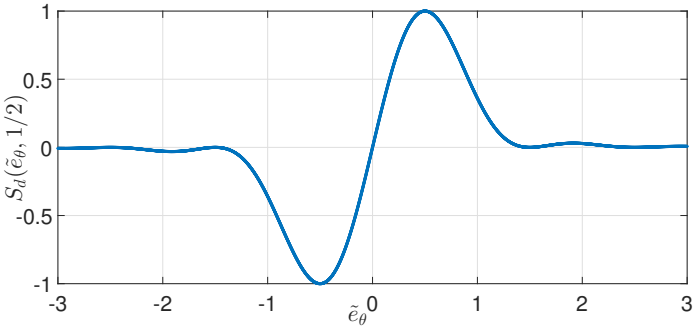

Fig. 2. Discriminator function of the CRS signal.

In a noise-free environment, the point at which the discriminator function is zero represents the TOA. However, noise can move the zero crossing point as

$$\tilde{e}_\theta = \frac{N_{i,d}}{k_d},$$

where

$$k_d = \left. \frac{\partial D_i(\tilde{e}_\theta, \xi)}{\partial \tilde{e}_\theta} \right|_{\substack{\tilde{e}_\theta \approx 0 \\ \xi = 1/2}} = \frac{4\pi C \cos(\frac{\pi}{2M})}{M \left(\sin(\frac{\pi}{2M})\right)^3}.$$

Therefore, the open-loop error due to noise, which is called pseudorange error, is a random variable with zero-mean and variance

$$\sigma^2_{\tilde{e}_\theta} = \frac{\text{var}[N_{i,d}]}{k_d^2} \approx \frac{\pi^2}{128MC/N_0},$$

which is obtained by assuming $M \gg 1$ and carrier-to-noise ratio $C/N_0 \gg 1$ dB-Hz, and by defining the power spectral density of noise as $S_n(f) \triangleq N_0/2 = \sigma^2$. Fig. 3 represents the standard deviation of the pseudorange error as a function of C/N_0 for different values of N_c. The results show that the pseudorange error improves significantly by increasing the bandwidth of the LTE signal.

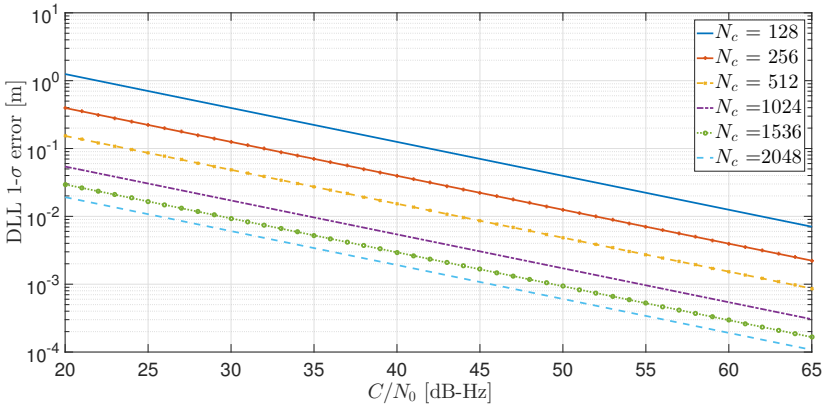

Fig. 3. Standard deviation of the pseudorange error as a function of the C/N_0 for a different number of subcarriers N_c.

The output of the discriminator function is first normalized by the slope of the S-curve, k_d, which represents the symbol timing error plus noise. Then, a DLL loop filter is used to achieve zero steady-state error. It can be assumed that the symbol timing error has linear variations, which can be due to the clock drift or receiver movement, and a second-order loop filter can provide zero steady-state error. Therefore, the normalized output of the discriminator function is first smoothed using a first-order low-pass filter (LPF) with a transfer function given by

$$F_{\text{DLL}}(s) = 1.414\,\omega_{n,d} + \frac{\omega^2_{n,d}}{s},$$

where $\omega_{n,d}$ is the undamped natural frequency of the delay loop, which can be related to the DLL noise-equivalent bandwidth $B_{n,\text{DLL}}$ by $B_{n,\text{DLL}} = 0.53\,\omega_{n,d}$ [34]. The output of the filter, which is the rate of change of the symbol timing error expressed in s/s, is then accumulated to update the frame start time estimate according to

$$\hat{e}_{\theta_{k+1}} = \hat{e}_{\theta_k} + \frac{T_{sub}}{T_s}\, v_{DLL},$$

where $\hat{e}_{\theta_k}$ is the k-th frame normalized symbol timing error estimate, $T_{sub} = 10$ ms is the subaccumulation period, and v_{DLL} is the output of the filter. Finally, the integer part of the frame start time estimate is used to control the FFT window and the fractional part is removed using the phase rotation in R_i.

IV. EXPERIMENTAL RESULTS

To evaluate the performance of the proposed receiver, an experiment was conducted using a ground vehicle in an urban multipath environment: downtown Riverside, California. In this section, the experimental setup and results are discussed.

A. Experimental Setup

In this experiment, a ground vehicle was equipped with two consumer-grade 800/1900MHz cellular omnidirectional Laird antennas to receive the LTE signals at 739 MHz and 1955 MHz carrier frequencies. These frequencies are used by the U.S. LTE provider AT&T. A dual-channel National Instruments (NI) universal software radio peripheral (USRP)-2954R driven by a GPS-disciplined oscillator (GPSDO) was used to simultaneously down-mix and synchronously sample LTE signals with 20 Msps. The vehicle was also equipped with one surveyor-grade Leica antenna to receive GPS signals. The

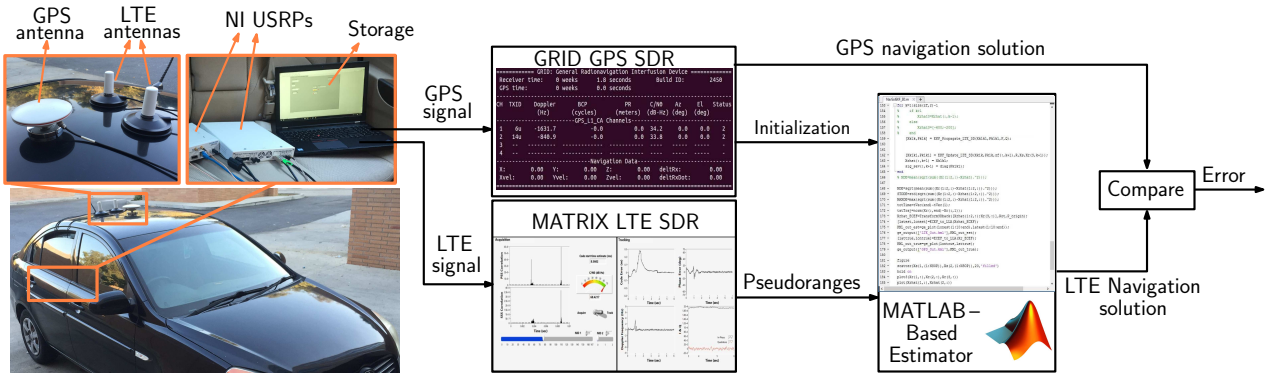

Fig. 4. Experimental hardware and software setup.

GPS signal, which was down-mixed and sampled by a single-channel NI USRP-2930, was used to discipline the USRP clock oscillators, and samples of the GPS signal were stored and later used to produce the vehicle "ground truth." A laptop was used to store the GPS and LTE signals for post-processing. Fig. 4 shows the experimental setup.

After collecting the LTE and GPS samples along the vehicle's trajectory, the stored LTE signals were processed using the proposed Multichannel Adaptive TRansceiver Information eXtractor (MATRIX) LTE SDR to obtain the pseudoranges. The GPS signal was processed using the generalized radionavigation interfusion (GRID) SDR [35]. An extended Kalman filter (EKF) was used to obtain the navigation solution using the navigation framework discussed in [19]. The GPS navigation solution was used to initialize the EKF states. Finally, the navigation solution obtained by the LTE SDR was compared against the GPS navigation solution, which was assumed to be the ground truth.

The characteristics of the eNodeBs to which the receiver was listening during the experiment are presented in Table I. The position of the eNodeBs were mapped prior to the experiment.

TABLE I
CHARACTERISTICS OF THE ENODEBS

eNodeB	Carrier frequency (MHz)	N_{ID}^{Cell}	Bandwidth (MHz)	Number of antennas
1	739	152	10	2
2	1955	216	20	2
3	739	232	10	2
4	739	288	10	2

B. Experimental Results

Over the course of the experiment, the ground vehicle traversed a trajectory of 1.44 Km in 90 s with an average speed of 16 m/s. The obtained pseudoranges with the proposed LTE SDR for each eNodeB is shown in Fig. 5(a) with dashed lines. The receiver had access to its actual position using the stored GPS signal. Therefore, the actual ranges of the receiver to each eNodeB can be obtained and is shown in Fig. 5(a) with solid lines. For the purpose of comparison, the initial values of the pseudoranges and actual ranges are removed in Fig. 5(a). It can be seen that the change in pseudoranges follows the actual ranges closely.

Fig. 5(b) shows the relative errors between the pseudoranges and their corresponding ranges. In this figure, it was assumed that the mean of each error is due to the difference of the clock biases between the receiver and the transmitter. Therefore, the mean of the obtained errors for each eNodeB was removed from the entire error, and the plotted errors have zero-mean. The results show that the standard deviation of the pseudorange errors for eNodeBs 1 to 4 are 6.2, 2.38, 4.11, and 7.37 m, respectively. The difference in the obtained standard deviations can be attributed to several factors, including: (1) different transmission bandwidth, (2) different multipath environment, and (3) different clock drifts.

Fig. 6(a) shows the distance error between the navigation solution obtained by the LTE SDR and that of the GPS navigation solution over time. The experimental cumulative distribution function (CDF) of the error is shown in Fig. 6(b). A summary of the LTE navigation performance is summarized in Table II.

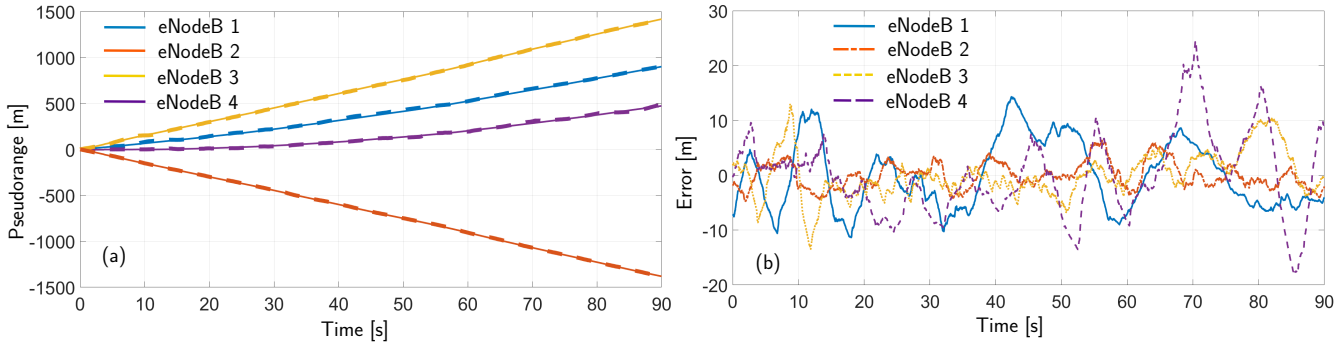

Fig. 5. (a) Measured pseudoranges and actual ranges for each eNodeB, which are plotted with dashed and solid lines, respectively. The initial values were removed for comparison purposes. (b) Obtained error between the pseudoranges and the actual ranges. The means of the errors, which show the difference of the clock biases of the receiver and each eNodeB, are removed.

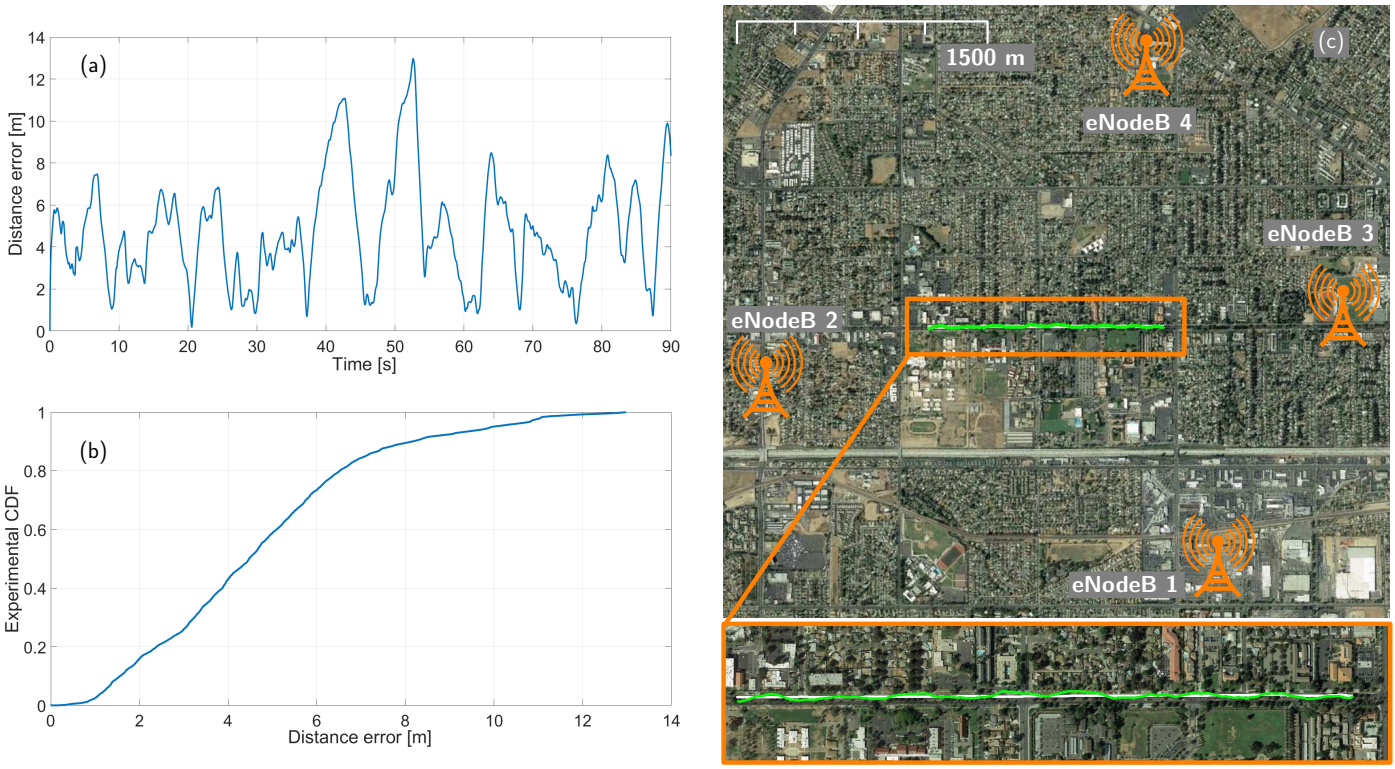

Fig. 6. (a) Distance error between the navigation solution obtained by the LTE SDR and the GPS navigation solution over time. (b) The CDF of the error. (c) Environment layout, the eNodeBs locations and the traversed trajectory. The results showed RMSE of 5.36 m, with the standard deviation of 2.54 m, and the maximum error of 12.97 m. Image: Google Earth.

TABLE II
LTE NAVIGATION PERFORMANCE

Performance Measure	Value
Root mean squared error (RMSE)	5.36 m
Standard deviation	2.54 m
Maximum error	12.97 m

C. Comparison with Other Methods

In this subsection, the performance of the proposed method is compared with the ESPRIT and EKAT algorithms discussed in [29]. The ESPRIT algorithm is known to provide highly accurate TOA estimation. However, this method needs perfect

knowledge of the channel impulse response length, L, to provide accurate results. Minimum description length (MDL) method is an approach that can be used to estimate L; but, this method tends to overestimate the channel length. As a result, the ESPRIT TOA estimation has an outlier. The effect of these outliers can be reduced significantly using a Kalman filter and a predetermined threshold on the vehicle's speed, which is called EKAT in [29]. Fig. 7 shows the pseudoranges obtained by the ESPRIT, EKAT, and the proposed receiver for all the eNodeBs. It can be seen that the pseudoranges obtained by ESPRIT have significant outliers, which is improved in EKAT. The pseudoranges shown in Fig. 7 are obtained using the same parameters as [29]. It can be seen that the pseudoranges obtained by the proposed receiver are significantly more robust and accurate.

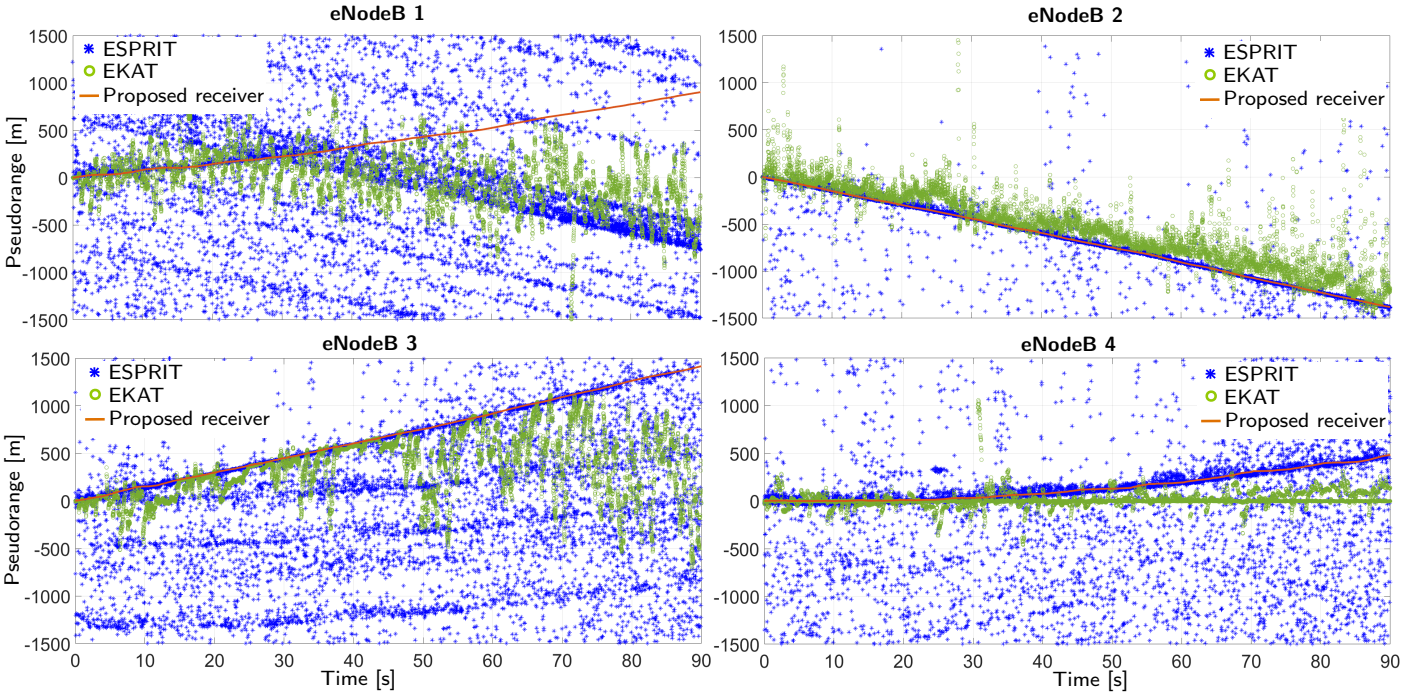

Fig. 7. Estimated pseudoranges obtained by the proposed receiver, ESPRIT, and EKAT algorithms for all the eNodeBs.

In terms of complexity, the ESPRIT and EKAT algorithms have complexity on the order of $O(N_c^3)$, which is mainly due to the singular value decomposition (SVD) operator. However, the complexity of the proposed receiver on in the order of $O(N_c \log N_c)$, which is due to the FFT operator.

V. CONCLUSION

This paper presented a low-cost, robust, and accurate receiver design for navigating exclusively with LTE signals in multipath environments. A brief review on the LTE signals structure and the ranging signals was first presented. The structure of the proposed receiver was presented. Experimental results comparing the navigation solutions obtained from GPS versus LTE utilizing the proposed receiver was provided. The experimental results showed an RMSE of 5.36 m, a standard deviation of 2.54 m, and a maximum error of 12.97 m over a 1.44 Km trajectory. Finally, the proposed receiver's performance was compared with the ESPRIT and EKAT algorithms, demonstrating robust and accurate pseudoranges with a significantly lower computational cost.

ACKNOWLEDGMENT

This work was supported in part by the Office of Naval Research (ONR) under Grant N00014-16-1-2305.

References

[1] S. Saab and Z. Kassas, "Power matching approach for GPS coverage extension," *IEEE Transactions on Intelligent Transportation Systems*, vol. 7, no. 2, pp. 156–166, June 2006.

[2] J. Du and M. Barth, "Next-generation automated vehicle location systems: Positioning at the lane level," *IEEE Transactions on Intelligent Transportation Systems*, vol. 9, no. 1, pp. 48–57, March 2008.

[3] R. Toledo-Moreo, D. Betaille, and F. Peyret, "Lane-level integrity provision for navigation and map matching with GNSS, dead reckoning, and enhanced maps," *IEEE Transactions on Intelligent Transportation Systems*, vol. 11, no. 1, pp. 100–112, March 2010.

[4] J. McEllroy, "Navigation using signals of opportunity in the AM transmission band," Master's thesis, Air Force Institute of Technology, Wright-Patterson Air Force Base, Ohio, USA, 2006.

[5] S. Fang, J. Chen, H. Huang, and T. Lin, "Is FM a RF-based positioning solution in a metropolitan-scale environment? A probabilistic approach with radio measurements analysis," *IEEE Transactions on Broadcasting*, vol. 55, no. 3, pp. 577–588, September 2009.

[6] P. Thevenon, S. Damien, O. Julien, C. Macabiau, M. Bousquet, L. Ries, and S. Corazza, "Positioning using mobile TV based on the DVB-SH standard," *NAVIGATION, Journal of the Institute of Navigation*, vol. 58, no. 2, pp. 71–90, 2011.

[7] K. Pesyna, Z. Kassas, and T. Humphreys, "Constructing a continuous phase time history from TDMA signals for opportunistic navigation," in *Proceedings of IEEE/ION Position Location and Navigation Symposium*, April 2012, pp. 1209–1220.

[8] Z. Kassas, "Collaborative opportunistic navigation," *IEEE Aerospace and Electronic Systems Magazine*, vol. 28, no. 6, pp. 38–41, 2013.

[9] Z. Kassas, "Analysis and synthesis of collaborative opportunistic navigation systems," Ph.D. dissertation, The University of Texas at Austin, USA, 2014.

[10] J. Khalife, Z. Kassas, and S. Saab, "Indoor localization based on floor plans and power maps: Non-line of sight to virtual line of sight," in *Proceedings of ION GNSS Conference*, September 2015, pp. 2291–2300.

[11] Z. Kassas, J. Morales, K. Shamaei, and J. Khalife, "LTE steers UAV," *GPS World Magazine*, vol. 28, no. 4, pp. 18–25, April 2017.

[12] Z. Kassas, J. Khalife, K. Shamaei, and J. Morales, "I hear, therefore I know where I am: Compensating for GNSS limitations with cellular signals," *IEEE Signal Processing Magazine*, pp. 111–124, September 2017.

[13] C. Yang, T. Nguyen, and E. Blasch, "Mobile positioning via fusion of mixed signals of opportunity," *IEEE Aerospace and Electronic Systems Magazine*, vol. 29, no. 4, pp. 34–46, April 2014.

[14] J. Khalife, K. Shamaei, and Z. Kassas, "A software-defined receiver architecture for cellular CDMA-based navigation," in *Proceedings of IEEE/ION Position, Location, and Navigation Symposium*, April 2016, pp. 816–826.

[15] J. Morales, P. Roysdon, and Z. Kassas, "Signals of opportunity aided inertial navigation," in *Proceedings of ION GNSS Conference*, September 2016, pp. 1492–1501.

[16] J. Morales, J. Khalife, and Z. Kassas, "Collaborative autonomous vehicles with signals of opportunity aided inertial navigation systems," in *Proceedings of ION International Technical Meeting Conference*, January 2017, 805–818.

[17] J. Morales, J. Khalife, and Z. Kassas, "GNSS vertical dilution of precision reduction using terrestrial signals of opportunity," in *Proceedings of ION International Technical Meeting Conference*, January 2016, pp. 664–669.

[18] J. Morales, J. Khalife, and Z. Kassas, "Opportunity for accuracy," *GPS World Magazine*, vol. 27, no. 3, pp. 22–29, March 2016.

[19] K. Shamaei, J. Khalife, and Z. Kassas, "Comparative results for positioning with secondary synchronization signal versus cell specific reference signal in LTE systems," in *Proceedings of ION International Technical Meeting Conference*, January 2017, pp. 1256–1268.

[20] J. del Peral-Rosado, J. Lopez-Salcedo, G. Seco-Granados, F. Zanier, and M. Crisci, "Preliminary analysis of the positioning capabilities of the positioning reference signals of 3GPP LTE," in *Proceedings of European Workshop on GNSS signals and Signal Processing*, December 2011.

[21] J. del Peral-Rosado, J. Lopez-Salcedo, G. Seco-Granados, F. Zanier, and M. Crisci, "Achievable localization accuracy of the positioning reference signal of 3GPP LTE," in *Proceedings of International Conference on Localization and GNSS*, June 2012, pp. 1–6.

[22] J. del Peral-Rosado, J. Lopez-Salcedo, G. Seco-Granados, F. Zanier, and M. Crisci, "Evaluation of the LTE positioning capabilities under typical multipath channels," in *Proceedings of Advanced Satellite Multimedia Systems Conference and Signal Processing for Space Communications Workshop*, September 2012, pp. 139–146.

[23] K. Shamaei, J. Khalife, and Z. Kassas, "Ranging precision analysis of LTE signals," in *Proceedings of European Signal Processing Conference*, August 2017, pp. 2788–2792.

[24] J. del Peral-Rosado, J. Lopez-Salcedo, G. Seco-Granados, F. Zanier, P. Crosta, R. Ioannides, and M. Crisci, "Software-defined radio LTE positioning receiver towards future hybrid localization systems," in *Proceedings of International Communication Satellite Systems Conference*, October 2013, pp. 14–17.

[25] J. del Peral-Rosado, J. Parro-Jimenez, J. Lopez-Salcedo, G. Seco-Granados, P. Crosta, F. Zanier, and M. Crisci, "Comparative results analysis on positioning with real LTE signals and low-cost hardware platforms," in *Proceedings of Satellite Navigation Technologies and European Workshop on GNSS Signals and Signal Processing*, December 2014, pp. 1–8.

[26] K. Shamaei, J. Khalife, and Z. Kassas, "Performance characterization of positioning in LTE systems," in *Proceedings of ION GNSS Conference*, September 2016, pp. 2262–2270.

[27] F. Knutti, M. Sabathy, M. Driusso, H. Mathis, and C. Marshall, "Positioning using LTE signals," in *Proceedings of Navigation Conference in Europe*, April 2015, pp. 1–8.

[28] F. Pittino, M. Driusso, A. Torre, and C. Marshall, "Outdoor and indoor experiments with localization using LTE signals," in *Proceedings of European Navigation Conference*, May 2017, pp. 311–321.

[29] M. Driusso, F. Babich, F. Knutti, M. Sabathy, and C. Marshall, "Estimation and tracking of LTE signals time of arrival in a mobile multipath environment," in *Proceedings of International Symposium on Image and Signal Processing and Analysis*, September 2015, pp. 276–281.

[30] M. Driusso, C. Marshall, M. Sabathy, F. Knutti, H. Mathis, and F. Babich, "Vehicular position tracking using LTE signals," *IEEE Transactions on Vehicular Technology*, vol. 66, no. 4, pp. 3376–3391, April 2017.

[31] R. Roy and T. Kailath, "ESPRIT-estimation of signal parameters via rotational invariance techniques," *IEEE Transactions on Acoustics, Speech, and Signal Processing*, vol. 37, no. 7, pp. 984–995, July 1989.

[32] 3GPP, "Evolved universal terrestrial radio access (E-UTRA); physical channels and modulation," 3rd Generation Partnership Project (3GPP), TS 36.211, January 2011. [Online]. Available: http://www.3gpp.org/ftp/Specs/html-info/36211.htm

[33] B. Yang, K. Letaief, R. Cheng, and Z. Cao, "Timing recovery for OFDM transmission," *IEEE Journal on Selected Areas in Communications*, vol. 18, no. 11, pp. 2278–2291, November 2000.

[34] E. Kaplan and C. Hegarty, *Understanding* GPS*: Principles and Applications*, 2nd ed. Artech House, 2005.

[35] T. Humphreys, J. Bhatti, T. Pany, B. Ledvina, and B. O'Hanlon, "Exploiting multicore technology in software-defined GNSS receivers," in *Proceedings of ION GNSS Conference*, September 2009, pp. 326–338.